Waste Management 128 (2021) 36–44

Contents lists available at ScienceDirect

Waste Management

journal homepage: www.elsevier.com/locate/wasman

Detailed nature of tire pyrolysis oil blended with light cycle oil and its hydroprocessed products using a NiW/HY catalyst

Roberto Palos [a], Timo Kekäläinen [b], Frank Duodu [b], Alazne Gutiérrez [a], José M. Arandes [a], Janne Jänis [b], Pedro Castaño [a,c]

[a] Chemical Engineering Department, University of the Basque Country UPV/EHU, P.O. Box 644-48080, Bilbao, Spain
[b] Department of Chemistry, University of Eastern Finland, PO Box 111, FI-80101, Joensuu, Finland
[c] Multiscale Reaction Engineering, KAUST Catalysis Center (KCC), King Abdullah University of Science and Technology (KAUST), Thuwal 23955-6900, Saudi Arabia

ARTICLE INFO

Article history:
Received 10 March 2021
Revised 12 April 2021
Accepted 17 April 2021

Keywords:
Tires
Pyrolysis oil
Hydroprocessing
Hydrocracking
FT-ICR/MS

ABSTRACT

The pyrolysis of scrap tires is a very attractive strategy to valorize chemically these end-of-life wastes. The products of this step and any additional one, such as hydrotreating, are relatively complex in nature entangling the understanding and limiting the viability. In this work, we have investigated in detail the composition of a tire pyrolysis oil blended with light cycle oil (from a refinery) and its hydrotreated products using a bifunctional NiW/HY catalyst at 320–400 °C. We have applied a set of analytical techniques to assess the composition, namely simulated distillation, ICP, GC/FID-PFPD, GC × GC/MS, and APPI FT-ICR/MS. Our results show the strength of our analytical workflow to highlight the compositional similarities of this pyrolysis oil with the standard refinery streams. The main differences arise from the higher boiling point species (originated during the pyrolysis of tires) and relatively high concentration of oxygenates. These effects can be minimized by hydrotreating the feed which effectively removes heteroatomic compounds from the feed while boosting the quantity and quality of gasoline and diesel fractions.

© 2021 Elsevier Ltd. All rights reserved.

1. Introduction

The concerns for depletion of petroleum resources, global warming and climate change have prompted scientific community to research in renewable and alternative energy resources (Hussain et al., 2017). Among the possible alternative resources that can be used to obtain energy, the valorization of consumer society wastes into energy carriers appears as a promising route to simultaneously reduce the environmental issues derived from their mismanagement (Palos et al., 2021). In this context, end-of-life (EOL) tires are one of the consumer goods that can definitely be used as an alternative energy source given their generation rate (ca. 17 million tons per year) (Arabiourrutia et al., 2020) and high energy content (about 30 MJ kg^{-1}) (Lopez et al., 2017). Furthermore, their uncontrolled dumping and landfill disposal may cause huge environmental damage, such as groundwater pollution and high level of hazardous emissions (carbon dioxide, methane, sulfur and nitrous oxides) if they burn in an uncontrollable manner (Machin et al., 2017).

Assessing the different technologies proposed for the valorization of EOL tires, pyrolysis is regarded as a promising route as it allows for obtaining high-value added products minimizing the environmental impact (Saab et al., 2020). Three different product fractions are obtained in the pyrolysis of EOL tires (Hita et al., 2016a): (i) a gas fraction mainly composed of hydrogen, light paraffins and olefins; (ii) a liquid fraction commonly known as tire pyrolysis oil (TPO); and (iii) a solid fraction or char that can be a source of activated carbon. As tires are typically vulcanized in order to improve their physicochemical and mechanical properties, pyrolysis products, especially TPO, are very complex and heterogeneous mixtures (Sathiskumar and Karthikeyan, 2019). Thus, TPO involves a wide range of hydrocarbons (from C6 to C50) and a considerable amount of heteroatomic molecules (S, N and O) and polyaromatic hydrocarbons. In order to improve the quality of the obtained TPO, many rectors have been proposed for its production (Lewandowski et al., 2019). In this line, catalytic pyrolysis offers greater selectivity to TPO and higher quality products (Luo et al., 2021). Additionally, catalytic hydro-pyrolysis offers even greater advantages in terms of product composition (Wang et al., 2019), but at the price of using big amounts of hydrogen without an efficient incorporation of it in the hydrocarbon stream.

In spite of the chemical composition of the TPO that advises against burning it directly, its use in internal combustion engines has received considerable attention in the literature (Karagöz

https://doi.org/10.1016/j.wasman.2021.04.041
0956-053X/© 2021 Elsevier Ltd. All rights reserved.

et al., 2020; Zhang et al., 2021). Hence, the use of neat TPO in internal combustion engines increases the emissions of particulate matter, smoke, CO, SO_X and NO_X comparing to diesel (Uyumaz et al., 2019). Consequently, different strategies have been proposed in order to overcome these poor results that consist of blending the TPO with diesel (İlkılıç and Aydın, 2011; Umeki et al., 2016), adding diethyl ether as an additive (Hariharan et al., 2013) and tailoring the injection strategies to optimize the behavior of the engine (Vihar et al., 2017).

Therefore, the most reasonable strategy appears to treat it as an intermediate refinery stream and use the well-known technology of the widespread and already depreciated refinery units for the upgrading of the TPO (Palos et al., 2021). Among the refinery units available, fluid catalytic cracking (FCC) unit offers good results in matter of conversion (Rodríguez et al., 2019a, 2019b). But, even co-feeding it with the current feedstock of FCC unit (vacuum gasoil), a subsequent mild hydroprocessing stage is required to adapt its composition to legislative requirements (Rodríguez et al., 2020). On the other hand, TPO can be directly treated in the hydroprocessing unit following a two-stage strategy: (i) the first stage with transition metal-based catalysts (Hita et al., 2016c, 2015a) in order to reduce the content of heteroatoms; and (ii) the second stage with precious metal-based catalysts (Hita et al., 2016b, 2015b) to fine-tune the composition of the final products. Furthermore, TPO can be co-fed with light cycle oil (LCO) to the hydroprocessing unit (Palos et al., 2019b) without causing any operational issue and affecting the quality of obtained products, easing its valorization and its upgrading within the structure of the refinery.

Nevertheless, TPO is a very complex mixture of organic compounds and to ensure that a proper upgrading is performed, high-resolution analytical methods are required to characterize both the TPO and obtained products. For instance, the nature of the heaviest compounds in TPO have been investigated using laser desorption ionization (LDI) combined with Fourier-transform ion cyclotron resonance mass spectrometry (FT-ICR/MS) (Rathsack et al., 2014). It allowed them to identify polyaromatic hydrocarbons together with different sulfur, nitrogen and oxygen containing structures with high degree of unsaturation, which are difficult to separate and detect by chromatographic means. Similarly, different works in the literature have resorted to these innovative characterization methods to unravel the complexity of the heavy fractions in oil-derived streams (Alawani et al., 2020; Ballard et al., 2020; Santos et al., 2020; Wang et al., 2020). This way, the improved knowledge acquired about the composition of both the feed and the obtained products will undoubtedly help to tailor the conditions of the upgrading stages and even the physicochemical properties of the catalysts used in the process.

In this context, the aim of this work was to clarify the composition of all fractions involved in TPO and its hydroprocessing products. In order to do so, we first obtained TPO from the pyrolysis of EOL tires in a conical spouted bed reactor. Then, the TPO was blended with LCO, which is a side product of the FCC unit, and was further hydrotreated using NiW/HY catalyst under moderate hydroprocessing conditions. The blend and products were then characterized by a set of techniques including gas chromatography (GC) with several detectors, bi-dimensional gas chromatography connected in-line with a mass spectrometer (GC × GC/MS) and ultrahigh-resolution FT-ICR/MS combined with atmospheric-pressure photoionization (APPI), which is suitable to target heavier hydrocarbons present in oil samples. Our multi-technique approach has shown to be very valuable to get a faithful compositional picture of the upgraded products from EOL tires exposing the strengths and weaknesses of the catalyst and of tested operating conditions.

2. Materials and methods

2.1. Hydrocarbon streams

A batch of light cycle oil (LCO), which is a side product of the fluid catalytic cracking unit, produced in the facilities of Petronor Refinery located in Muskiz (Spain) has been used as current hydrotreating unit feedstock. Its main physicochemical properties and composition have been determined in the previous work (Palos et al., 2018) and there have been collected in Table S1 in the Supplementary Material. Briefly, LCO consists of a diesel boiling range stream (initial and final boiling points of 95.7–438.0 °C, respectively) with high contents of aromatics (62.1 wt%) and sulfur-containing compounds (10212 ppm).

End-of-life tires pyrolysis oil (TPO) was obtained through the flash pyrolysis of discarded tires at 500 °C in a pilot scale plant equipped with a conical spouted bed reactor. A detailed explanation of the plant used for the production of the TPO can be found elsewhere (Lopez et al., 2017). Typical characteristics for such untreated pyrolysis oil used in the current work can be found in Table S1 in the Supplementary Material. In short, the obtained TPO has a broader boiling range than LCO (initial and final boiling points of 109.4–537.9 °C, respectively) lower content of aromatics (56.2 wt%) and higher of sulfur-containing compounds (11200 ppm).

2.2. Catalyst

A commercial catalyst based on NiW/USY extrudates has been used for this process. Prior to be used, the catalyst has been crushed and sieved to the desired particle size (150–300 μm). Moreover, a detailed characterization of the NiW/USY catalyst has been performed in order to correlate its features with its properties. Obtained results have been summarized in Table 1. Physical properties have been obtained by means of N_2 adsorption-desorption isotherms in a Micromeritics ASAP 2010 apparatus, whereas chemical composition has been determined by Inductively coupled plasma atomic emission spectroscopy (ICP-AES) with an X7-II Thermo Elemental quadrupole mass spectrometer (Q-ICP-MS). Total acidity and acid strength have been obtained using temperature programmed desorption (TPD) of previously adsorbed *tert*-butylamine (t-BA) in a TG-DSC Setaram 111 calorimeter provided with a Harvard Apparatus syringe and connected in-line with a Balzers Quadstar 422 mass spectrometer to track the number of desorbed amines. Finally, Brønsted/Lewis acid sites ratio has been determined by Fourier transform infrared (FTIR) analysis in a Thermo Nicolet 6700 using pyridine as probe molecule.

Table 1
Main physicochemical properties of the NiW/USY catalyst.

	NiW/USY
Physical properties	
BET surface area ($m^2\ g^{-1}$)	317
Mesopore volume ($cm^3\ g^{-1}$)	0.082
Average pore diameter (Å)	43
Chemical composition	
NiO (wt%)	4.54
WO_3 (wt%)	22.7
Si/Al ratio	0.31
Catalytic properties	
Total acidity ($mmol_{t\text{-}BA}\ g^{-1}$)	0.405
Acid strength ($kJ\ mol^{-1}_{t\text{-}BA}$)	511
Brønsted/Lewis acid sites ratio	2.39

2.3. Catalytic tests

The catalytic tests have been carried out in a PID Tech Microactivity-Pro equipment provided with a packed bed reactor located inside a heated oven (Fig. S1). The feed has consisted of a TPO/LCO blend composed of 20 wt% of TPO and 80 wt% of LCO. This ratio has been established taking into account the average capacity of hydrotreating units for these fractions (40000 b/d) and the TPO that can be generated considering the EOL tires produced (192 ktons in Spain that can be converted into 116 ktons of TPO assuming a liquid yield of 60 wt% in the pyrolysis stage). Indeed, co-feeding 20 wt% TPO in hydrotreaters is a very ambitious goal but we have used this value for assessing its effects in the overall process scheme. The operation conditions have been the following: 320 and 400 °C; pressure, 80 bar; H_2:Feed ratio, 1000 mL_{NC} mL^{-1}; weight hourly space velocity (WHSV), 5 h^{-1}; and time on stream (TOS), 8 h. The catalyst has been mixed with silicon carbide and placed between two silicon carbide beds in the reactor, in order to ensure plug flow regime and to avoid temperature gradients and preferential paths along the catalyst bed (van Herk et al., 2009). Moreover, before reaction the catalyst has been sulfided in situ at 400 °C for 4 h under a continuous flow of 50 mL min^{-1} of H_2S/H_2 (10 vol%).

2.4. Bulk chemical analysis

An Elementar GmbH vario Micro Cube V1.7 instrument has been used for elemental analysis. The amounts of carbon, hydrogen and sulfur have been directly determined using CO_2, H_2O and SO_2 detectors, respectively, whereas the amount of nitrogen has been determined with a thermal conductivity detector (TCD). The amount of oxygen has been computed by difference. Finally, the CHNOS content has been determined on a dry basis by subtracting the water content.

Water content of the samples has been measured according to the method for water using volumetric Karl Fischer titration described in ASTM E203 Standard. The analyses have been performed with a Metrohm 870 KF Titrino Plus titrator using Hydranal Composite 5 K as a titration agent.

Acidic constituents of the TPO/LCO blend and of the obtained products have been determined by semi-micro color indicator titration according to the method described in ASTM D3339 Standard. The analyses have been carried out with an SI Analytics Titronic universal titrator. Briefly, the samples have been dissolved in a solvent composed of isopropanol (495 mL), toluene (500 mL) and water (5 mL). The sample size used has been of 0.1 g for the feed and of 0.6 g for the products to correspond better with the typical total acid number (TAN) values of pyrolysis oils. Afterwards, obtained solution has been titrated at a temperature below 30 °C with the standardized 0.01 M potassium hydroxide titrant and using *p*-naphtholbenzein as indicator.

2.5. GC × GC/MS analysis

GC × GC/MS analysis has been carried out using an Agilent 5976C TAD Series Gas Chromatograph/Mass Selective Detector System combined with an Agilent 7890A GC. An automatic sampler (Agilent Technologies 7683B series) provided with a 10 μL syringe has been used as a sample injection system. The GC is equipped with two capillary columns, which are connected by means of a flow-modulator: (i) a non-polar DB-5 MS J&W 122–5532 (length, 30 m; inner diameter, 0.25 mm; film thickness, 0.25 μm) in the first dimension; and (ii) a polar HP-INNOWAX (length, 5 m; inner diameter, 0.25 mm; film thickness, 0.15 μm) in the second dimension. The samples have been injected at 300 °C in a 150:1 split ratio. The oven temperature has been programmed from 40 to 260 °C following a heating rate of 10 °C min^{-1} and held for 25 min. The interface temperature to the mass spectrometer has been set at 280 °C, whereas ion source has been heated at 230 °C. The MS has been operated at a scan speed of 12,500 amu s^{-1} covering a range of *m*/*z* 35–500.

2.6. GC/FID-PFPD analysis

Speciation of the sulfur-containing compounds has been done in a gas chromatograph (Agilent Technologies, model 7890A) equipped with both FID (flame ionization detector) and PFPD (pulsed flame photometric detector) detectors and fitted with a HP-PONA capillary column (length, 50 m; inner diameter, 0.20 mm; film thickness, 0.50 μm). Helium has been used as carrier under a constant flow of 0.85 mL min^{-1}. The sample volume injected has been of 0.3 μL, which has been injected by means of an autosampler (Agilent Technologies 6850 ALS GC). The GC oven temperature has been set at 40 °C for 3 min and then heated at 15 °C min^{-1} to 235 °C, and maintained for 1 min. Next, the oven has been heated again following a 30 °C min^{-1} heating rate to 320 °C and maintained for 20 min. The temperature of FID and PFPD detectors has been set at 320 and 340 °C, respectively, whereas the injector temperature has been 250 °C.

Simulated distillation analyses have been performed following the procedure described on ASTM D2887 Standard in an Agilent Technologies 6890 GC System, which is equipped with an FID detector and a DB-2887 semicapillary column (length, 10 m; inner diameter, 0.53 mm; film thickness, 3 μm). A constant flow of 9.4 mL min^{-1} of hydrogen has been used for carrying purposes. The sample (0.2 μL) has been manually injected in the GC using a Hamilton 7000 series Microliter syringe. The oven temperature has been programmed as follows: 40 °C (hold for 5 min), heated up to 125 °C with a rate of 10 °C min^{-1}, then heated at 5 °C min^{-1} to 150 °C and 10 °C min^{-1} to 300 °C, and held constant for 30 min. FID detector has been heated at 320 °C and the injector at 350 °C.

2.7. FT-ICR MS analysis

APPI FT-ICR MS experiments have been performed on a 12-T Bruker solariX XR instrument (Bruker Daltonics), equipped with an Apollo-II atmospheric-pressure photoionization source, operating in positive-ion APPI mode, and a dynamically harmonized ICR cell (ParaCell). The oil samples have been prepared in methanol:toluene (1:1, v/v) solvent mixture to the concentration of 100 μg mL^{-1} and directly infused into the ion source at a flow rate of 7 μL min^{-1}. For each mass spectrum, 300 co-added 8 MWord time-domain transients have been summed, full-sine apodized and zero-filled once to provide final 16 MWord magnitude mode data (at *m*/*z* 100–2000). The external mass calibration has been done with an APCI-L tuning mix (Part No. G1969-85010, Agilent Technologies) and further internal recalibration with known homologous compounds present in TPO. The instrument has been controlled with ftmsControl 2.1 and the data post-processing and molecular formula assignments have been accomplished with DataAnalysis 5.0 software (Bruker Daltonics). A more detailed description of the instrument and the data analysis can be found elsewhere (Palos et al., 2019b).

3. Results

3.1. Bulk properties

The TPO/LCO blend and its hydrotreated products are composed of elemental C, H, O, N and S, together with small concentrations of diverse soluble inorganic elements, e.g., V, Ni, Fe, Cu and Co among

others. The results obtained from the elemental analysis of these samples have been collected in Table 2, where it can be seen that in all the cases C and H account for the 97–98 wt% of the composition. Moreover, as a consequence of the hydrotreating process, a higher H content has been obtained in the reaction products (10.46 and 11.03 wt% at 320 and 400 °C, respectively) than in the feed (10.27 wt%). Consequently, the H/C ratio of the feed (1.40) has been improved reaching values of 1.44 and 1.51 at 320 and 400 °C, respectively. Additionally, the content of the heteroatoms has decreased during hydrotreating and in a higher extent at 400 °C. The most remarkable reduction has been observed for S, which has decreased from 0.84 wt% in the feed to 0.36 wt% in the product obtained at 320 °C and has further decreased below the detection level of the apparatus at 400 °C. Likewise N followed a similar trend but does not reach such small values (0.19 and 0.16 wt% at 320 and 400 °C, respectively). In contrast, O did not respond to hydrotreating as the amount is higher or similar than in the feed. However, the quantification of oxygen is difficult as the value determined with a conventional CNHS analyzer also includes inorganics (oxygen calculated by difference), which may also be present in TPO.

Water is the final product of the direct hydrodeoxygenation reactions and its content in the reaction products could offer a fast idea of the hydrodeoxygenation (HDO) reaction extent (Cordero-Lanzac et al., 2017). However, oxygen can be also removed by means of decarbonylation and decarboxylation reactions leading to the formation of CO and CO_2 molecules, respectively (Arora et al., 2018). The content of water is higher in the feed (0.27 wt %) than in the reaction products and decreases with reaction temperature (0.21 and 0.16 wt% at 320 and 400 °C, respectively). Apparently, no direct-HDO reactions are occurring in the process as the content of water has been reduced. This is consistent with the CHNOS analysis (Table 2).

Finally, the TAN of the feed and the reaction products has been also determined. This parameter indicates the potential of corrosion problems that an oily sample may create, but it does not measure the corrosive nature of an oil (Laredo et al., 2004). This way, the TAN has been significantly reduced from 5.60 to 2.00 and 2.29 mg_{KOH} g^{-1} operating at 320 and 400 °C, respectively. The high value of the TAN of the TPO/LCO is typically attributed to the high content of naphthenic acids present in the TPO (Alvarez et al., 2017). Even though a remarkable improvement has been obtained, the products are still considered as highly acidic oils as their TAN is higher than 1.0 mg_{KOH} g^{-1} (Cho et al., 2020).

Overall, the results from the bulk analyses expose a notable improvement of the quality of the products obtained in the hydroprocessing process, specifically operating at 400 °C.

3.2. Monodimensional and bidimensional GC analysis

Simulated distillation analysis allows for characterizing petroleum-derived streams since it determines the boiling range distribution of the samples. According to the criteria commonly followed in refinery (Rodríguez et al., 2020), the feed and the products have been divided into three different fractions: (i) naphtha (<216 °C); (ii) diesel (216–343 °C); and (iii) gasoil (>343 °C). Thus, Fig. 1 depicts the simulated distillation curves obtained for the feed and the products. As it can be seen, the higher the reaction temperature, the lighter the products obtained. This result exposes the hydrocracking activity of the catalyst and the boosting of the cracking reactions at high temperatures, which is supported by its acidic properties (Table 1).

The extent of the hydrocracking activity is commonly assessed by computing the hydrocracking conversion, which is defined as the amount of gasoil that reacted divided by the amount of the gasoil that was fed (Cao et al., 2021). This way, the conversion level obtained at 320 °C has been of 40.3%, whereas it has reached the value of 76.6% at 400 °C. Attained conversion levels probe the suitability of the NiW/HY catalyst used, as important reductions of the gasoil fraction have been obtained without causing an excessive over-cracking of the lighter fractions.

Focusing on the fraction distribution, diesel is the main one in the TPO/LCO (65.4 vol%) and remains as the most important one in the products (59.3–54.3 vol% at 320 and 400 °C, respectively), in spite of the reduction suffered. On the other hand, the contents of gasoil and naphtha fractions are significantly modified. This way, naphtha increases from 19.2 vol% in the feed to 31.5 vol% in the products obtained at 320 °C, at the same time that gasoil fraction is reduced from 15.4 to 9.2 vol%. However, these changes in product fractions are clearly more significant at 400 °C, since the content of naphtha increases up to 42.1 vol% and that of gasoil is reduced to 3.6 vol%. This result is due to the higher hydrocracking activity at these conditions. Another important observation out of the results presented in Fig. 1 is related to the fact that none of the rest of the analytical techniques that will be described from this point are capable to analyze the feed as a whole. GC × GC/MS and GC/FID-PFPD techniques can analyze species with boiling points up to 340–400 °C, whereas APPI FT-ICR MS can detect species (more effectively) with boiling point higher than 200 °C. From this point onward, we will focus on the individual analysis of each of these techniques.

Fig. 2 compares the nature of the products obtained with the composition of the TPO/LCO blend. It can be seen that despite the fact that obtained products maintain the aromatic nature of

Table 2
Elemental analysis, water content and total acid number of the feed and reaction products.

	TPO/LCO	320 °C	400 °C
Elemental analysis (wt%)			
C	87.89 ± 0.37	87.17 ± 0.76	87.82 ± 0.87
H	10.27 ± 0.14	10.46 ± 0.11	11.03 ± 0.07
N	0.21 ± 0.05	0.19 ± 0.03	0.16 ± 0.03
S	0.84 ± 0.01	0.36 ± 0.05	not detected
O + inorganic elements	0.79 ± 0.45	1.82 ± 0.82	0.99 ± 0.93
H/C ratio	1.40	1.44	1.51
Water content (vol%)	0.27 ± 0.07	0.21 ± 0.04	0.16 ± 0.04
TAN (mg_{KOH} g^{-1})	5.60 ± 0.61	2.00 ± 0.02	2.29 ± 0.21

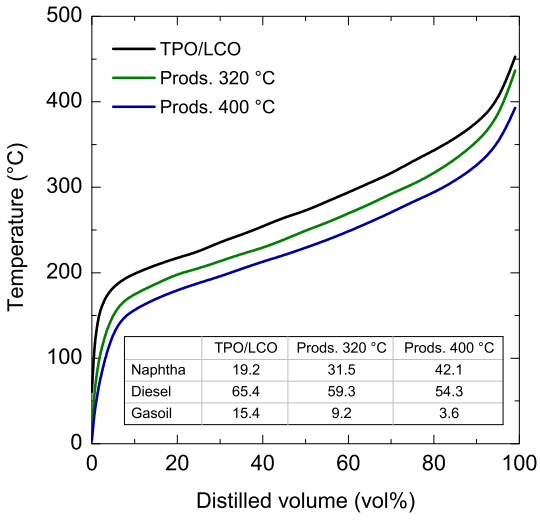

Fig. 1. Simulated distillation curves and boiling fractions distribution (in vol%) of the TPO/LCO blend and the products using the different hydrotreating conditions (320 and 400 °).

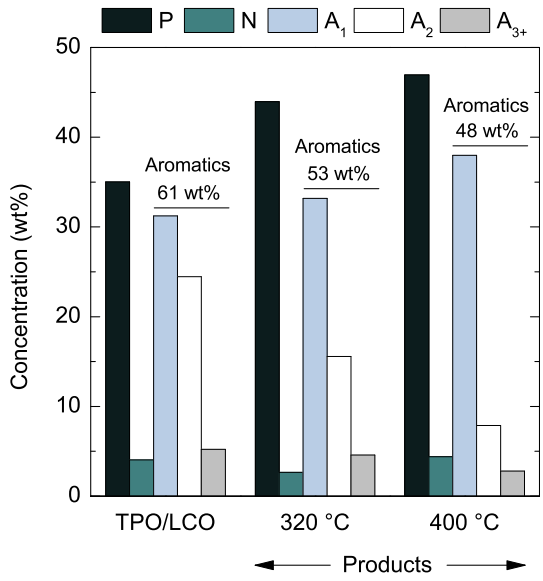

Fig. 2. Chemical nature and total content of aromatics obtained by GC × GC/MS, applied to the TPO/LCO blend and the products using the different hydrotreating conditions (320 and 400 °C).

the feedstock (61 wt%), the total content of aromatics is lower than that of the feed (53 and 48 wt% at 320 and 400 °C, respectively). With regard to their distribution, a substantial difference in the ease of the hydrogenation of monoaromatics and polyaromatics has been observed. This way, 3^+-ring aromatics are converted into 2-ring aromatics that are, in turn, hydrogenated to 1-ring aromatics. However, the saturation of monoaromatics to naphthenes occurs in lesser extent, which has previously proved kinetically (Kalenchuk et al., 2020). Consequently, the concentration of 1-ring aromatics increases from 31.2 wt% in the TPO/LCO blend to 33.2 and 38.0 at 320 and 400 °C, respectively. The saturation of the polyaromatics to monoaromatics observed by means of mild hydrogenation, converts the stock much more susceptible to be cracked down in a subsequent stage, such as a catalytic cracking stage in the FCC unit. Therefore, the reduction of the total content of aromatics and the subsequent increase of paraffins expose the activity of the catalyst for the cracking of aliphatic appendages and for the cleavage of the C–C bonds of the naphthenic rings (Galadima and Muraza, 2018). The reaction mechanism is a consequence of the thermal synergistic activation of the selective ring opening reactions, in which both metallic and acidic phases of the catalyst are involved (Galadima and Muraza, 2016). Brønsted acidic sites, present in the support (Table 1), activate the initial ring-contraction and protonation processes, leading to the formation of carbenium ions and liberating H_2 via protolytic dehydrogenation process. At the same time, metallic sites are crucial in the activation of hydrogenation, hydrogenolysis and isomerization reactions, since they promote the aforementioned catalytic processes that take place on the acidic sites.

Hydrodearomatization (HDA) conversion, defined as the amount of aromatics that disappeared divided by the initial total amount of aromatics (Fang et al., 2019), is also commonly computed to determine the extent of HDA reactions. Thus, the conversion values obtained at 320 and 400 °C have been of 13.1 and 21.3 wt%, respectively. The hydrogenation reactions of aromatics are highly exothermic reversible reactions, meaning that at high temperatures dehydrogenation or condensation reactions are favored instead of hydrogenation ones. Therefore, it should have been expected a higher HDA conversion level at 320 than at 400 °C. However, the aromatic hydrogenation equilibrium conversion reaches its maximum value at ca. 380 °C (Palos et al., 2019a), meaning that the deviation from the optimum temperature is lower at 400 °C.

The speciation of the sulfur-containing compounds of the TPO/LCO blend, together with that of the products obtained at 320 and 400 °C have been collected in Fig. 3. The initial sulfur concentration of the TPO/LCO blend is of 10410 ppm, with an important contribution of refractory species (4395 ppm). The sulfur content of the product obtained at 320 °C has been of 2245 ppm, which corresponds to a conversion level of 78 wt%, whereas at 400 °C a product with 222 ppm of sulfur has been obtained (conversion level of 97.8 wt%). These results expose the relevance of the reaction temperature on the desulfurization level reached. Taking into account that hydroprocessing aims the reduction of heteroatoms to avoid corrosion during refining and to improve burning characteristics of the fuels, the sulfur content in the reaction products should be reduced below 250 ppm. Thus, just the product obtained at 400 °C reaches the desired desulfurization level.

The different reactivity of the families of sulfur-containing compounds found in the TPO/LCO blend is clearly appreciable in Fig. 3. On the one hand, the benzothiazole present in the feedstock (733 ppm) is completely removed in the whole range of studied operating conditions, since it is not detected in the products. Moreover, it can be seen that benzothiophene and its alkyl-derivatives (5282 ppm in the feedstock) are very reactive, as they are only detected in the reaction products obtained at 320 °C (632 ppm), being totally removed at 400 °C. On the other hand, dibenzothiophene and its alkyl-derivatives (4395 ppm in the feedstock) are more refractory, since the sulfur content detected in the product obtained at 400 °C is solely composed of these types of compounds. This clear difference in the reactivity of the different families of sulfur-containing compounds has already been observed before (Hita et al., 2016c, 2015a) in the hydroprocessing of TPO dissolved in decane with NiMo-based catalysts.

3.3. High-resolution APPI FT-ICR MS analysis

The number of species detected in the TPO/LCO blend and its two hydrotreating products is shown in Fig. 4a. Moreover, they have been divided in the different compound classes detected, namely, CH (hydrocarbon classes), S_x (sulfur classes), N_y (nitrogen

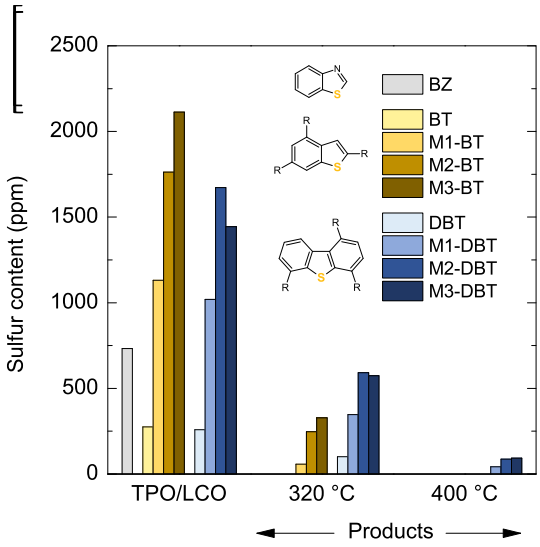

Fig. 3. Speciation of the sulfur-containing compounds obtained by GC/PFPD, applied to the TPO/LCO blend and the products using the different hydrotreating conditions (320 and 400 °C).

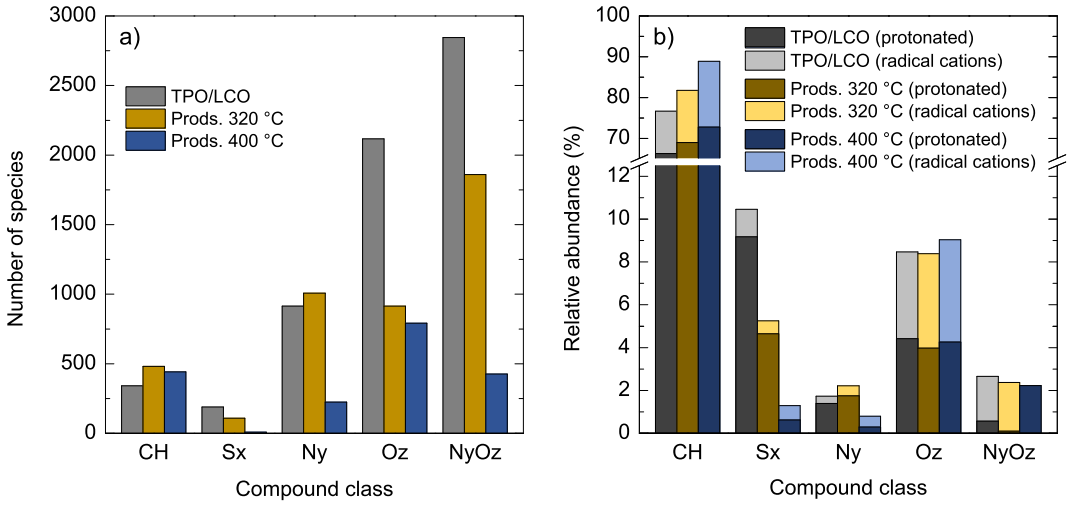

Fig. 4. Distribution of the different compound classes according to their number of species (a) and relative abundance (b) obtained by APPI FT-ICR MS, applied to the TPO/LCO blend and the products using the different hydrotreating conditions (320 and 400 °C).

classes), O_z (oxygen classes) and N_yO_z (nitrogen and oxygen classes). The number of species detected in the feed (6406 species) is higher than that detected in the products obtained at 320 and 400 °C (4373 and 1892 species, respectively). Hence, hydroprocessing has notably modified the composition of the feedstock, which is more evident attending to the distribution of the different compound classes. Moreover, in comparison of two hydroprocessing temperatures, these classes have shown different removal patterns. The N_yO_z classes has been mainly removed at 400 °C, since it has decreased from 2845 species in the feed to 1860 and 426 in the products obtained at 320 and 400 °C, respectively. On the contrary, the O_z classes are significantly reduced at 320 °C (from 2116 to 915 species), while increasing the temperature further to 400 °C has shown only a small additional effect (791 species). The N_y classes, in turn, are influenced by the removal of the N_yO_z classes. This way, the number of species that belong to this class is higher in the products obtained at 320 °C than in the feed (1008 and 915 species, respectively). This increase can be attributed to the removal of the O atoms of the compounds that initially belonged to N_yO_z classes, which end being part of the N_y classes. However, at 400 °C an important reduction of the number of species of N_y classes has been obtained. On the other hand, the number of species that belong to S_x classes are gradually reduced with temperature from 189 in the feed to 109 and 8 species at 320 and 400 °C, respectively. Finally, CH classes are strongly influenced by the removal of heteroatoms and by the cracking activity of the catalyst. This way, the higher number of species has been detected at 320 °C (481 species), which is reduced at 400 °C (442 species) because of the boosting of the cracking reactions.

However, attending to the relative abundances of all the classes (Fig. 4b) a totally different reading of obtained results can be done. Firstly, it can be seen that hydrocarbon class compounds dominate both the feed and the products, while the relative abundances of heteroatoms are clearly lower. The abundance of S_x classes changed from 10.5% in the feed to 5.3 and 1.3% after being hydroprocessed at 320 and 400 °C, respectively. In total, the relative abundance has been reduced in a 87.6% at the harshest conditions. Meanwhile, the abundance of the N_y classes goes through a maximum at 320 °C and reaches its minimum value at 400 °C, as ocurred with the number of species belonging to these classes (Fig. 4a). However, the reduction attained (42.2%) did not reach the same magnitude as that observed for S_x classes. The relative abundances of N_yO_z classes also decrease with temperature reaching a value of zero at 400 °C in the protonated analyte molecules. Finally, the O_z classes display only the minor modification of all the compund classes, since it goes from 4.42% in the feed to 3.98 and 4.26% at 320 and 400 °C, respectively. Therefore, the relative abundance change during hydroprocessing exposes that the hydro-removal capacity of heteroatoms follows the order of S > N > O (Campuzano et al., 2020).

To obtain a more detailed picture on the chemistry of the heteroatoms, van Krevelen-type plots have been generated for the most abundant heteroatom classes, namely S_1, N_1 and O_1 classes (Fig. 5). These diagrams cross-plot the hydrogen:carbon (H/C) atomic ratio as a function of the heteroatom:carbon atomic ratio, namely, sulfur (S/C), nitrogen (N/C) and oxygen (O/C) (Fig. 5a-c, d-e and g-i, respectively). Additionally, the relative abundance of each species has been color-coded as indicated in each subgraph. Focusing on the distribution of the S_1 compound class (Fig. 5a-c), an increase of the temperature (from 320 to 400 °C) is directly related to the decrease of detected S_1 species and of their relative abundance, which was the expected behavior (Bakhshi Ani et al., 2015).

A great variety of sulfur-containing compounds has been detected in the feed (Fig. 5a). Indeed, the point cloud goes from values of 0.5 to 1.95 in the H/C atomic ratio and from 0.025 to 0.125 in the S/C atomic ratio. The main families of compounds have been benzothiophenes (BT), dibenzothiophenes (DBT) and naphtobenzothiophenes (NBT). In the hydroprocessed samples, an important reduction for most of the sulfur species has been achieved. At 320 °C, a narrower point cloud has been obtained (Fig. 5b), in which the compounds with higher H/C and S/C atomic ratios have been removed. On the contrary, the compounds that belong to DBT and NBT families remain almost unchanged exposing their well-known refractory character (Guillemant et al., 2020a) and the limitations of the catalyst to hydrogenate the aromatic rings of these molecules (Liu et al., 2021). A more efficient sulfur removal has been achieved at 400 °C, as it can be seen in Fig. 5c. This is evident for BT and NBT that have been hardly detected, while some residual species of DBT are still present. Once again, the promotion of the hydrodesulfurization activity of the catalyst at high temperatures has been exposed. Furthermore, attending to the high sulfur removal rate reached and the poor hydrogenation activity of the catalyst (Fig. 2), it can be concluded that the direct desulfurization

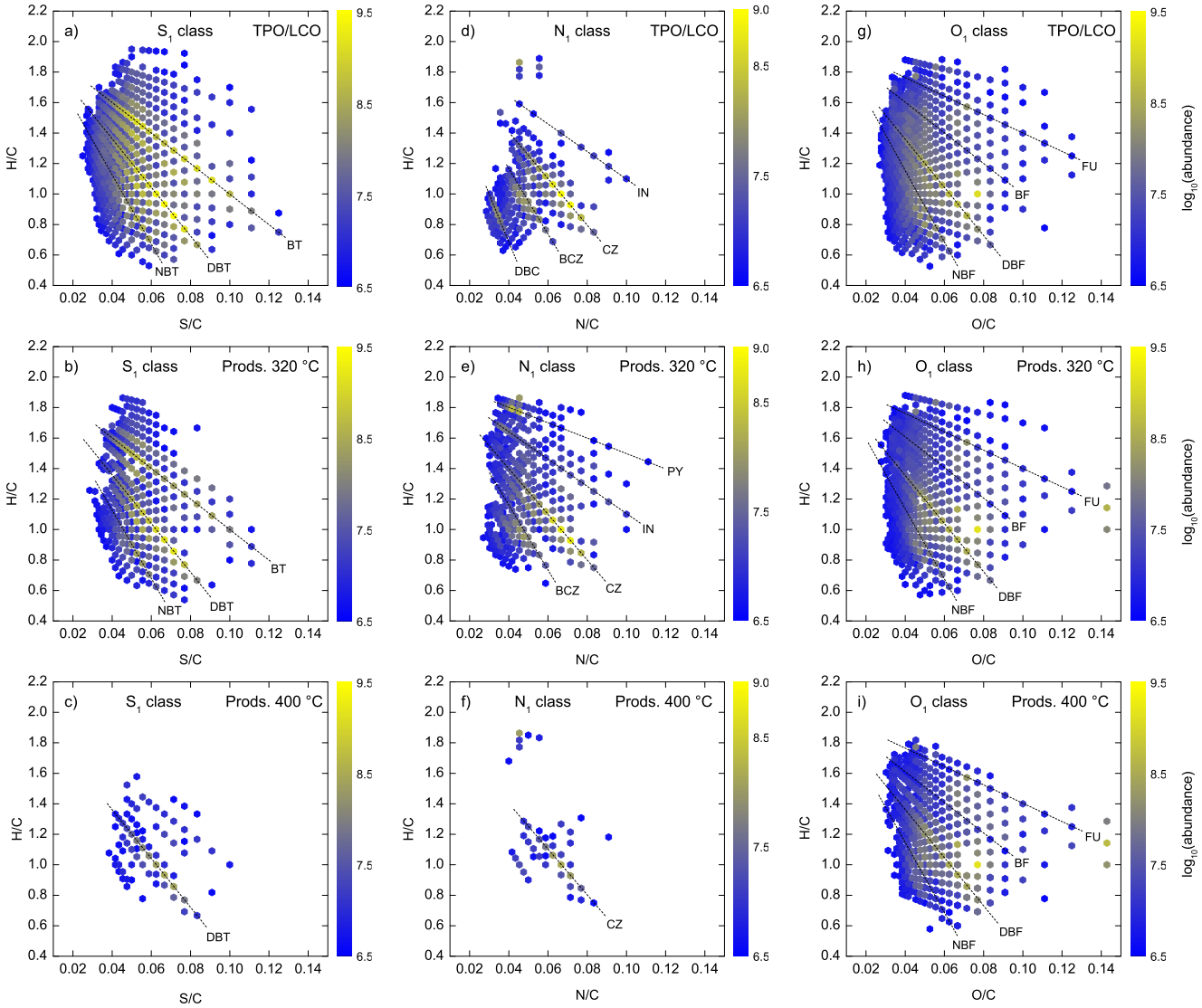

Fig. 5. Iso-abundance plots of H/C atomic ratio versus heteroatom:carbon atomic ratio, namely, sulfur (S/C), nitrogen (N/C) and oxygen (O/C) (a-c, d-f and g-i, respectively) obtained by APPI FT-ICR MS, applied to the TPO/LCO blend and the products using the different hydrotreating conditions (320 and 400 °C).

route is the predominant one, since the indirect one requires a prior hydrogenation of the aromatic rings (Escobar et al., 2017).

Nitrogen compounds (N_1) distribution has been collected in Fig. 5d-f. A wide distribution of this family of compounds has been detected in the feed (Fig. 5d) with a point cloud ranging from 0.6 to 1.9 and from 0.03 to 0.10 in the H/C and N/C atomic ratios, respectively. Attending to their relative abundance, the following sub-families have been detected among the nitrogen compounds: indoles (IN), carbazoles (CZ), benzocarbazoles (BCZ) and dibenzocarbazoles (DBC). Even though petroleum derivative streams are composed of both basic and non-basic nitrogen compounds, which are directly related to pyridine and pyrrole derivatives, respectively, the most abundant sub-families detected are all non-basic. This was an expectable result as the ratio of non-basic to basic nitrogen compounds in petroleum fractions is commonly within the 2.85–4.0 range (Xia et al., 2021). On the other hand, a wider and more intense point cloud has been detected in the product hydroprocessed at 320 °C (Fig. 5e). This phenomenon has been also observed before (Guillemant et al., 2020b) in the hydrotreatment of vacuum gasoil and is a consequence of the contribution of compounds from other families such as N_2, N_1S_1, N_1O_1 or N_1O_3, in which their heteroatoms are just partially removed. In addition, the cracking and hydrogenation of heavy molecules has led to the formation of lighter nitrogen species. Furthermore, since the breaking of a C–N bond requires prior heterocyclic ring hydrogenation and ring opening (Nguyen et al., 2017), a new sub-family of compounds has appeared as one of the most intense: pyrroles (PY). Finally, the distribution of the nitrogen compounds obtained at 400 °C has been displayed in Fig. 5f. Overall, all the nitrogen containing compounds have been notably reduced obtaining a much narrower distribution. Among the main sub-families detected, the one that remained in the products is that of CZ, exposing the refractory character of these molecules, which is accentuated by the steric hindrance produced by high alkylation degrees (Guillemant et al., 2019). Moreover, some compounds with high values of H/C (ca. 1.8) and low values of N/C (ca. 0.05) atomic ratios remain in the products. These compounds consist of long chain nitriles that are obtained in the ring opening and cracking of BCZ, CZ and IN.

Oxygen compounds are not very common in petroleum-derived feeds, but they are present in the oils obtained in the pyrolysis of EOL tires (Campuzano et al., 2021). Thus, the O_1 species observed

in the feed (Fig. 5g) can be mostly attributed to the TPO included in the blend. As indicated in the graphs, four main sub-species have been detected this time: furanes (FU), benzofuranes (BF), dibenzofuranes (DBF) and naphtobenzofuranes (NBF). Regarding the evolution of the distribution pattern, it can be seen that minor reductions of O_1 species have occurred during hydroprocessing stages. In spite of the pattern narrowing and of the intensity reduction, all the main sub-species detected in the feed remained in the products (Fig. 5h and i). Indeed, DBF are dominant in both the feed and the reaction products given their highly refractory character. Comparing the pattern of the products with that of the feedstock, it can be seen that NBF are hydrogenated and resulted in an upward movement of H/C ratios, especially at 400 °C. Compounds with high H/C and O/C values have been partially removed at 320 °C, but totally removed at 400 °C. This result exposes that low condensed furanic species are more likely to be removed than highly condensed ones (Ni et al., 2018).

4. Conclusions

The multi-technique analytical workflow investigated in this work can satisfactorily describe the composition of the oils derived from the pyrolysis of tires and its hydrotreated product. We treated the pyrolysis oil blended with a secondary interest refinery stream: light cycle oil from the fluid catalytic cracking unit. This analytical workflow includes simulated distillation, elemental analysis, advanced gas chromatography (mono- and bidimensional), and high-resolution mass spectrometry.

The main compositional singularities of the tire pyrolysis oils are (1) the high concentration of heteroatomic molecules and the (2) wide distribution of boiling points, driven by the unselective tire pyrolysis process per-se and given that it is not a distillation fraction. The distribution of heteroatomic molecules in terms of sulfur, nitrogen and oxygen is nominally similar than any other refinery stream, such as light cycle oil, except for the presence of benzothiazole which is removed very easily by hydrotreating.

Our results clearly show that both heteroatomic and high boiling point molecules are removed by the co-hydrotreating with light cycle oil. We demonstrated that the hydrotreatment at 400 °C, 80 bar and with a NiW/USY catalyst enables to obtain 96.4 wt% middle distillates (gasoline and diesel) with significantly high quality. These results, point to the fact that tires and tire oils are great candidates for being used in refinery schemes with high carbon utilization and waste management capabilities, so called the waste refinery.

CRediT authorship contribution statement

Roberto Palos: Conceptualization, Investigation, Writing-original draft, visualization, Writing-review & editing. **Timo Kekäläinen**: Investigation, Writing-review & editing. **Frank Duodu**: Investigation, Writing-review & editing. **Alazne Gutiérrez**: Conceptualization, Investigation, Writing-review & editing. **José M. Arandes**: Supervision, Funding acquisition, Writing-review & editing. **Janne Jänis**: Supervision, Funding acquisition, Writing-review & editing. **Pedro Castaño**: Conceptualization, Writing- review & editing, Supervision, Project administration.

Declaration of Competing Interest

The authors declare that they have no known competing financial interests or personal relationships that could have appeared to influence the work reported in this paper.

Acknowledgements

This work has been carried out with the financial support of the Ministry of Science, Innovation and Universities (MICIU) of the Spanish Government (grant RTI2018-096981-B-I00), the European Union's ERDF funds and Horizon 2020 Research and Innovation Programme under the Marie Skłodowska-Curie and INFRAIA actions (grants 823745 and 731077) and the Basque Government (grant IT1218-19). Dr. Roberto Palos thanks the University of the Basque Country UPV/EHU for his postdoctoral grant (UPV/EHU 2019). Funding for this work was provided by King Abdullah University of Science and Technology (KAUST). The FT-ICR/MS facility is supported by Biocenter Kuopio/Biocenter Finland and the ERDF (grant A70135). The authors also thank Taina Nivajärvi for a skillful technical assistance.

Appendix A. Supplementary data

Supplementary data to this article can be found online at https://doi.org/10.1016/j.wasman.2021.04.041.

References

Alawani, N.A., Muller, H., Panda, S.K., Al-Hajji, A.A., Koseoglu, O.R., 2020. Evaluation of polycyclic aromatic hydrocarbon removal from hydrocracking recycle streams. Energy Fuels 34 (1), 179–187. https://doi.org/10.1021/acs.energyfuels.9b0338210.1021/acs.energyfuels.9b03382.s001.

Alvarez, J., Lopez, G., Amutio, M., Mkhize, N.M., Danon, B., van der Gryp, P., Görgens, J.F., Bilbao, J., Olazar, M., 2017. Evaluation of the properties of tyre pyrolysis oils obtained in a conical spouted bed reactor. Energy 128, 463–474. https://doi.org/10.1016/j.energy.2017.03.163.

Arabiourrutia, M., Lopez, G., Artetxe, M., Alvarez, J., Bilbao, J., Olazar, M., 2020. Waste tyre valorization by catalytic pyrolysis – A review. Renew. Sustain. Energy Rev. 129, 109932. https://doi.org/10.1016/j.rser.2020.109932.

Arora, P., Ojagh, H., Woo, J., Lind Grennfelt, E., Olsson, L., Creaser, D., 2018. Investigating the effect of Fe as a poison for catalytic HDO over sulfided NiMo alumina catalysts. Appl. Catal. B Environ. 227, 240–251. https://doi.org/10.1016/j.apcatb.2018.01.027.

Bakhshi Ani, A., Ale Ebrahim, H., Azarhoosh, M.J., 2015. Simulation and multi-objective optimization of a trickle-bed reactor for diesel hydrotreating by a heterogeneous model using non-dominated sorting genetic algorithm II. Energy Fuels 29 (5), 3041–3051. https://doi.org/10.1021/acs.energyfuels.5b00467.

Ballard, D.A., Chacón-Patiño, M.L., Qiao, P., Roberts, K.J., Rae, R., Dowding, P.J., Xu, Z., Harbottle, D., 2020. Molecular characterization of strongly and weakly interfacially active asphaltenes by high-resolution mass spectrometry. Energy Fuels 34 (11), 13966–13976. https://doi.org/10.1021/acs.energyfuels.0c0275210.1021/acs.energyfuels.0c02752.s001.

Campuzano, F., Abdul Jameel, A.G., Zhang, W., Emwas, A.-H., Agudelo, A.F., Martínez, J.D., Sarathy, S.M., 2021. On the distillation of waste tire pyrolysis oil: A structural characterization of the derived fractions. Fuel 290,. https://doi.org/10.1016/j.fuel.2020.120041 120041.

Campuzano, F., Abdul Jameel, A.G., Zhang, W., Emwas, A.-H., Agudelo, A.F., Martínez, J.D., Sarathy, S.M., 2020. Fuel and chemical properties of waste tire pyrolysis oil derived from a continuous twin-auger reactor. Energy Fuels 34 (10), 12688–12702. https://doi.org/10.1021/acs.energyfuels.0c02271.

Cao, Z., Zhang, X., Xu, C., Huang, X., Wu, Z., Peng, C., Duan, A., 2021. Selective hydrocracking of light cycle oil into high-octane gasoline over bi-functional catalysts. J. Energy Chem. 52, 41–50. https://doi.org/10.1016/j.jechem.2020.04.055.

Cho, K., Rana, B.S., Cho, D.-W., Beum, H.T., Kim, C.-H., Kim, J.-N., 2020. Catalytic removal of naphthenic acids over Co-Mo/γ-Al_2O_3 catalyst to reduce total acid number (TAN) of highly acidic crude oil. Appl. Catal. A Gen. 606, 117835. https://doi.org/10.1016/j.apcata.2020.117835.

Cordero-Lanzac, T., Palos, R., Arandes, J.M., Castaño, P., Rodríguez-Mirasol, J., Cordero, T., Bilbao, J., 2017. Stability of an acid activated carbon based bifunctional catalyst for the raw bio-oil hydrodeoxygenation. Appl. Catal. B Environ. 203, 389–399. https://doi.org/10.1016/j.apcatb.2016.10.018.

Escobar, J., Barrera, M.C., Gutiérrez, A.W., Terrazas, J.E., 2017. Benzothiophene hydrodesulfurization over NiMo/alumina catalysts modified by citric acid. Effect of addition stage of organic modifier. Fuel Process. Technol. 156, 33–42. https://doi.org/10.1016/j.fuproc.2016.09.028.

Fang, D., Wang, G., Sheng, Q., Ge, S., Gao, C., Gao, J., 2019. Preparation of hydrogen donor solvent for asphaltenes efficient liquid-phase conversion via heavy cycle oil selective hydrogenation. Fuel 257, 115886. https://doi.org/10.1016/j.fuel.2019.115886.

Galadima, A., Muraza, O., 2018. Hydrocracking catalysts based on hierarchical zeolites: A recent progress. J. Ind. Eng. Chem. 61, 265–280. https://doi.org/10.1016/j.jiec.2017.12.024.

Galadima, A., Muraza, O., 2016. Ring opening of hydrocarbons for diesel and aromatics production: Design of heterogeneous catalytic systems. Fuel 181, 618–629. https://doi.org/10.1016/j.fuel.2016.05.024.

Guillemant, J., Albrieux, F., OliveiraDe, L.P., Lacoue-nègre, M., Joly, J., 2019. Insights from nitrogen compounds in gas oils highlighted by high-resolution Fourier transform mass spectrometry. Anal. Chem. 91 (20), 12644–12652. https://doi.org/10.1021/acs.analchem.9b01702.

Guillemant, J., Berlioz-Barbier, A., Chainet, F., de Oliveira, L.P., Lacoue-Nègre, M., Joly, J.-F., Duponchel, L., 2020a. Sulfur compounds characterization using FT-ICR MS: Towards a better comprehension of vacuum gas oils hydrodesulfurization process. Fuel Process. Technol. 210, 106529. https://doi.org/10.1016/j.fuproc.2020.106529.

Guillemant, J., Berlioz-Barbier, A., de Oliveira, L.P., Albrieux, F., Lacoue-Nègre, M., Duponchel, L., Joly, J.-F., 2020b. Exploration of the reactivity of heteroatomic compounds contained in vacuum gas oils during hydrotreatment using Fourier transform ion cyclotron resonance mass spectrometry. Energy Fuels 34 (9), 10752–10761. https://doi.org/10.1021/acs.energyfuels.0c0176010.1021/acs.energyfuels.0c01760.s001.

Hariharan, S., Murugan, S., Nagarajan, G., 2013. Effect of diethyl ether on tyre pyrolysis oil fueled diesel engine. Fuel 104, 109–115. https://doi.org/10.1016/j.fuel.2012.08.041.

Hita, I., Arabiourrutia, M., Olazar, M., Bilbao, J., Arandes, J.M., Castaño, P., 2016a. Opportunities and barriers for producing high quality fuels from the pyrolysis of scrap tires. Renew. Sustain. Energy Rev. 56, 745–759. https://doi.org/10.1016/j.rser.2015.11.081.

Hita, I., Cordero-Lanzac, T., Gallardo, A., Arandes, J.M., Rodríguez-Mirasol, J., Bilbao, J., Cordero, T., Castaño, P., 2016b. Phosphorus-containing activated carbon as acid support in a bifunctional Pt-Pd catalyst for tire oil hydrocracking. Catal. Commun. 78, 48–51. https://doi.org/10.1016/j.catcom.2016.01.035.

Hita, I., Gutiérrez, A., Olazar, M., Bilbao, J., Arandes, J.M., Castaño, P., 2015a. Upgrading model compounds and Scrap Tires Pyrolysis Oil (STPO) on hydrotreating NiMo catalysts with tailored supports. Fuel 145, 158–169. https://doi.org/10.1016/j.fuel.2014.12.055.

Hita, I., Palos, R., Arandes, J.M., Hill, J.M., Castaño, P., 2016c. Petcoke-derived functionalized activated carbon as support in a bifunctional catalyst for tire oil hydroprocessing. Fuel Process. Technol. 144, 239–247. https://doi.org/10.1016/j.fuproc.2015.12.030.

Hita, I., Rodríguez, E., Olazar, M., Bilbao, J., Arandes, J.M., Castaño, P., 2015b. Prospects for Obtaining High Quality Fuels from the Hydrocracking of a Hydrotreated Scrap Tires Pyrolysis Oil. Energy Fuels 29 (8), 5458–5466. https://doi.org/10.1021/acs.energyfuels.5b01181.

Hussain, A., Arif, S.M., Aslam, M., 2017. Emerging renewable and sustainable energy technologies: State of the art. Renew. Sustain. Energy Rev. 71, 12–28. https://doi.org/10.1016/j.rser.2016.12.033.

İlkılıç, C., Aydın, H., 2011. Fuel production from waste vehicle tires by catalytic pyrolysis and its application in a diesel engine. Fuel Process. Technol. 92 (5), 1129–1135. https://doi.org/10.1016/j.fuproc.2011.01.009.

Kalenchuk, A., Bogdan, V., Dunaev, S., Kustov, L., 2020. Influence of steric factors on reversible reactions of hydrogenation-dehydrogenation of polycyclic aromatic hydrocarbons on a Pt/C catalyst in hydrogen storage systems. Fuel 280,. https://doi.org/10.1016/j.fuel.2020.118625 118625.

Karagöz, M., Ağbulut, Ü., Sarıdemir, S., 2020. Waste to energy: Production of waste tire pyrolysis oil and comprehensive analysis of its usability in diesel engines. Fuel 275, 117844. https://doi.org/10.1016/j.fuel.2020.117844.

Laredo, G.C., López, C.R., Álvarez, R.E., Castillo, J.J., Cano, J.L., 2004. Identification of naphthenic acids and other corrosivity-related characteristics in crude oil and vacuum gas oils from a Mexican refinery. Energy Fuels 18 (6), 1687–1694. https://doi.org/10.1021/ef034004b.

Lewandowski, W.M., Januszewicz, K., Kosakowski, W., 2019. Efficiency and proportions of waste tyre pyrolysis products depending on the reactor type—A review. J. Anal. Appl. Pyrolysis 140, 25–53. https://doi.org/10.1016/j.jaap.2019.03.018.

Liu, X., Li, L., Sun, H., Wen, G., Wang, D., Ren, S., Guo, Q., Zhang, W., He, S., Shen, B., 2021. NiW catalyst modified with C12A7-H− and its promotion to hydrogenation selectivity of hydrodesulfurization. Fuel 290, 120037. https://doi.org/10.1016/j.fuel.2020.120037.

Lopez, G., Alvarez, J., Amutio, M., Mkhize, N.M., Danon, B., van der Gryp, P., Görgens, J.F., Bilbao, J., Olazar, M., 2017. Waste truck-tyre processing by flash pyrolysis in a conical spouted bed reactor. Energy Convers. Manag. 142, 523–532. https://doi.org/10.1016/j.enconman.2017.03.051.

Luo, W., Wan, J., Fan, Z., Hu, Q., Zhou, N., Xia, M., Song, M., Qi, Z., Zhou, Z., 2021. In-situ catalytic pyrolysis of waste tires over clays for high quality pyrolysis products. Int. J. Hydrogen Energy 46 (9), 6937–6944. https://doi.org/10.1016/j.ijhydene.2020.11.170.

Machin, E.B., Pedroso, D.T., de Carvalho, J.A., 2017. Energetic valorization of waste tires. Renew. Sustain. Energy Rev. 68, 306–315. https://doi.org/10.1016/j.rser.2016.09.110.

Nguyen, M.-T., Tayakout-Fayolle, M., Chainet, F., Pirngruber, G.D., Geantet, C., 2017. Use of kinetic modeling for investigating support acidity effects of NiMo sulfide catalysts on quinoline hydrodenitrogenation. Appl. Catal. A Gen. 530, 132–144. https://doi.org/10.1016/J.APCATA.2016.11.015.

Ni, H., Xu, C., Wang, R., Guo, X., Long, Y., Ma, C., Yan, L., Liu, X., Shi, Q., 2018. Composition and transformation of sulfur-, oxygen-, and nitrogen- containing compounds in the hydrotreating process of a low- temperature coal tar. Energy Fuels 32 (3), 3077–3084. https://doi.org/10.1021/acs.energyfuels.7b0365910.1021/acs.energyfuels.7b03659.s001.

Palos, R., Gutiérrez, A., Arandes, J.M., Bilbao, J., 2018. Catalyst used in fluid catalytic cracking (FCC) unit as a support of NiMoP catalyst for light cycle oil hydroprocessing. Fuel 216, 142–152. https://doi.org/10.1016/j.fuel.2017.11.148.

Palos, R., Gutiérrez, A., Hita, I., Castaño, P., Thybaut, J.W., Arandes, J.M., Bilbao, J., 2019a. Kinetic modeling of hydrotreating for enhanced upgrading of light cycle oil. Ind. Eng. Chem. Res. 58 (29), 13064–13075. https://doi.org/10.1021/acs.iecr.9b0209510.1021/acs.iecr.9b02095.s001.

Palos, R., Gutiérrez, A., Vela, F.J., Olazar, M., Arandes, J.M., Bilbao, J., 2021. Waste refinery: The valorization of waste plastics and end-of-life tires in refinery units. A review. Energy Fuels 35 (5), 3529–3557. https://doi.org/10.1021/acs.energyfuels.0c03918.

Palos, R., Kekäläinen, T., Duodu, F., Gutiérrez, A., Arandes, J.M., Jänis, J., Castaño, P., 2019b. Screening hydrotreating catalysts for the valorization of a light cycle oil/scrap tires oil blend based on a detailed product analysis. Appl. Catal. B Environ. 256, 117863. https://doi.org/10.1016/j.apcatb.2019.117863.

Rathsack, P., Kroll, M., Rieger, A., Haseneder, R., Gerlach, D., Repke, J.-U., Otto, M., 2014. Analysis of high molecular weight compounds in pyrolysis liquids from scrap tires using Fourier transform ion cyclotron resonance mass spectrometry. J. Anal. Appl. Pyrolysis 107, 142–149. https://doi.org/10.1016/j.jaap.2014.02.014.

Rodríguez, E., Gutiérrez, A., Palos, R., Azkoiti, M.J., Arandes, J.M., Bilbao, J., 2019a. Cracking of Scrap Tires Pyrolysis Oil in a Fluidized Bed Reactor under Catalytic Cracking Unit Conditions. Effects of Operating Conditions. Energy Fuels 33 (4), 3133–3143. https://doi.org/10.1021/acs.energyfuels.9b0029210.1021/acs.energyfuels.9b00292.s001.

Rodríguez, E., Palos, R., Gutiérrez, A., Arandes, J.M., Bilbao, J., 2020. Scrap tires pyrolysis oil as a co-feeding stream on the catalytic cracking of vacuum gasoil under fluid catalytic cracking conditions. Waste Manag. 105, 18–26. https://doi.org/10.1016/j.wasman.2020.01.026.

Rodríguez, E., Palos, R., Gutiérrez, A., Arandes, J.M., Bilbao, J., 2019b. Production of non-conventional fuels by catalytic cracking of scrap tires pyrolysis oil. Ind. Eng. Chem. Res. 58 (13), 5158–5167. https://doi.org/10.1021/acs.iecr.9b0063210.1021/acs.iecr.9b00632.s001.

Saab, R., Polychronopoulou, K., Zheng, L., Kumar, S., Schiffer, A., 2020. Synthesis and performance evaluation of hydrocracking catalysts: A review. J. Ind. Eng. Chem. 89, 83–103. https://doi.org/10.1016/j.jiec.2020.06.022.

Santos, J.M., Vetere, A., Wisniewski, A., Eberlin, M.N., Schrader, W., 2020. Modified SARA method to unravel the complexity of resin fraction(s) in crude oil. Energy Fuels 34 (12), 16006–16013. https://doi.org/10.1021/acs.energyfuels.0c02833.

Sathiskumar, C., Karthikeyan, S., 2019. Recycling of waste tires and its energy storage application of by-products –a review. Sustain. Mater. Technol. 22, e00125. https://doi.org/10.1016/j.susmat.2019.e00125.

Umeki, E.R., de Oliveira, C.F., Torres, R.B., dos Santos, R.G., 2016. Physico-chemistry properties of fuel blends composed of diesel and tire pyrolysis oil. Fuel 185, 236–242. https://doi.org/10.1016/j.fuel.2016.07.092.

Uyumaz, A., Aydoğan, B., Solmaz, H., Yılmaz, E., Yeşim Hopa, D., Aksoy Bahtli, T., Solmaz, Ö., Aksoy, F., 2019. Production of waste tyre oil and experimental investigation on combustion, engine performance and exhaust emissions. J. Energy Inst. 92 (5), 1406–1418. https://doi.org/10.1016/j.joei.2018.09.001.

van Herk, D., Castaño, P., Quaglia, M., Kreutzer, M.T., Makkee, M., Moulijn, J.A., 2009. Avoiding segregation during the loading of a catalyst-inert powder mixture in a packed micro-bed. Appl. Catal. A Gen. 365 (1), 110–121. https://doi.org/10.1016/j.apcata.2009.06.003.

Vihar, R., Baškovič, U.Ž., Seljak, T., Katrašnik, T., 2017. Combustion and emission formation phenomena of tire pyrolysis oil in a common rail Diesel engine. Energy Convers. Manag. 149, 706–721. https://doi.org/10.1016/j.enconman.2017.02.005.

Wang, K., Xu, Y., Duan, P., Wang, F., Xu, Z.-X., 2019. Thermo-chemical conversion of scrap tire waste to produce gasoline fuel. Waste Manag. 86, 1–12. https://doi.org/10.1016/j.wasman.2019.01.024.

Wang, N., Zhi, Y., Wei, Y., Zhang, W., Liu, Z., Huang, J., Sun, T., Xu, S., Lin, S., He, Y., Zheng, A., Liu, Z., 2020. Molecular elucidating of an unusual growth mechanism for polycyclic aromatic hydrocarbons in confined space. Nat. Commun. 11, 1079. https://doi.org/10.1038/s41467-020-14493-9.

Xia, Y., Ma, C., Ju, R., Zhao, C., Zheng, F., Sun, X., Li, Z., Wang, C., Shi, D., Lin, X., Lu, X., Xu, G., 2021. Characterization of nitrogen-containing compounds in petroleum fractions by online reversed-phase liquid chromatography-electrospray ionization Orbitrap mass spectrometry. Fuel 284, 119035. https://doi.org/10.1016/j.fuel.2020.119035.

Zhang, G., Chen, F., Zhang, Y., Zhao, L., Chen, J., Cao, L., Gao, J., Xu, C., 2021. Properties and utilization of waste tire pyrolysis oil: A mini review. Fuel Process. Technol. 211, 106582. https://doi.org/10.1016/j.fuproc.2020.106582.